Quantifying the fractal dimension and morphology of individual atmospheric soot aggregates

Pang, Yuner; Wang, Yuanyuan; Wang, Zhicheng; Zhang, Yinxiao; Liu, Lei; Kong, Shaofei; Liu, Fengshan; Shi, Zongbo; Li, Weijun

DOI:
10.1029/2021JD036055

Quantifying the fractal dimension and morphology of individual atmospheric soot aggregates

Yuner Pang[1], Yuanyuan Wang[1], Zhicheng Wang[2], Yinxiao Zhang[1], Lei Liu[1], Shaofei Kong[3], Fengshan Liu[4], Zongbo Shi[5], Weijun Li[1]

[1] Key Laboratory of Geoscience Big Data and Deep Resource of Zhejiang Province, Department of Atmospheric Sciences, School of Earth Sciences, Zhejiang University, Hangzhou, 310027, China

[2]College of Control Science and Engineering, Zhejiang University, Hangzhou, 310027, China

[3]Department of Atmospheric Sciences, School of Environmental Studies, China University of Geosciences, Wuhan, 430074, China

[4]Metrology Research Centre, National Research Council of Canada, Ottawa, Ontario, Canada

[5]School of Geography, Earth and Environmental Sciences, University of Birmingham, Birmingham, U.K.

Corresponding author: Weijun Li (liweijun@zju.edu.cn)

Key Points:

- A novel image recognition technique is used to calculate the fractal dimension of individual soot particle based on electron microscope
- An aging process of soot particles collected at an urban tunnel is observed from the entrance to its exit
- The fractal dimension of soot particles from different sources is similar with that of urban site but lower than that of rural site

Abstract

The complex morphology of soot aggregates is a major source of uncertainty in evaluating their warming effects in the atmosphere. Fractal dimension (D_f) is a key parameter in quantifying the morphology of soot particles. Previous studies are mostly based on manual identification of soot monomers in electron microscopic images and are hard to provide comparable results in determination of D_f. Here we develop a novel image recognition technique to automatically determine the D_f of individual soot aggregates from electron microscopy images. The novel method has been shown to be able to trace the small change of the soot D_f from an urban tunnel (1.61±0.19) to its exit (1.70±0.15). By applying this new method, we show a substantial difference in average D_f of soot particles emitted from vehicles (1.66±0.17) than from biomass burning (1.75±0.18) and coal burning (1.76±0.18). Average D_f of soot from an urban atmosphere (1.77±0.18) is close to that from biomass and coal combustion but much lower than that from a rural atmosphere (1.85±0.13). In summary, the new technique provides an automatic, accurate and reliable quantification of soot morphology (D_f), enabling an improved understanding of soot aging processes and a more accurate modeling of soot impact on their climate.

Plain Language Summary

Soot particles play a significant role in global climate warming by affecting the radiative balance at both global and regional scales. A key challenge of evaluating the warming effects of soot particle is to quantify their complex morphology. We for the first time developed a novel image recognition technique to quantify the morphology of individual soot particles on electron microscopy and collected a large amount of soot particles from various combustion sources and ambient atmosphere. We compared the new method with previous methods and found aging process of soot particles from tunnel entrance to exit. Our results show substantial differences in the morphology of soot particles from different sources and allow us to better model the soot impact on the climate.

1 Introduction

Soot, also known as black carbon (BC), is a typical aerosol particle. It plays the major role of light-absorbing carbonaceous component of fine particles and forms during the incomplete combustion of biomass and fossil fuels (Bond et al., 2013). Soot particle has been considered as the second largest anthropogenic radiative forcer in the present-day climate after CO_2 (Boucher et al., 2013). It plays a significant role in global warming by affecting the radiative balance at both global and regional scales (Moffet & Prather, 2009; Peng et al., 2016; Ramanathan & Carmichael, 2008; Teng et al., 2019). Because of their light absorption capacity, a large number of soot particles in polluted air above the planetary layer (PBL) can depress the PBL height and further deteriorate surface air quality (Ding et al., 2016). Soot particles are also constitute of covalently bound clusters of polycyclic aromatic hydrocarbon (PAHs) and other hydrocarbons that contribute to soot surface growth and have detrimental impacts on human health and environment (Johansson et al., 2018; Pendergrass & Hartmann, 2012).

Individual soot particles display very complex morphological structures (Y. Y. Wang et al., 2017). Studies show that soot particles are chain-like aggregates that are composed of tens to thousands of nearly spherical monomers with diameters of 5-50 nm (China et al., 2013; Li et al., 2003) and a certain degree of overlap and necking between touching monomers (Figure 1). Up to now, it has remained a challenge to quantify the complex fractal morphology of individual soot particle (China et al., 2013; Ishimoto et al., 2019). Though we can visualize the real morpholoy of individual soot particles through various advanced electron microscopes, the lack of methods that efficiently quantify the fractal morphology directly from the electron microscopic images prevents the morphological data of real soot particles conversion to numerical shape models. However, the numerical shape models of soot particles are essential to accurately simulate their optical properties and quantify their climate effects in the atmospheric models (K. Adachi et al., 2007; van Poppel et al., 2005; Y. Wang et al., 2021b).

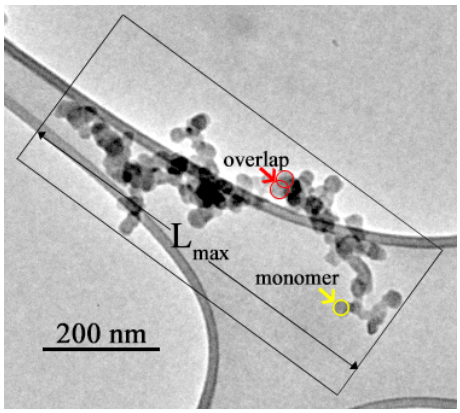

Figure 1. An example of a transmission electron microscope (TEM) image of one soot aggregate. The rather thick gray curving lines are the lacey carbon supporting substrates.

The fractal dimension (D_f) has been widely used as a key parameter to describe the fractal morphology of soot particles (Brasil et al., 1999; Oh & Sorensen, 1997) and the following three methods have been developed and applied to calculate the D_f of soot particles based on electron microscopic images in the past decades. The first one is the box counting method. This method can detect the boundary of individual soot particle but its computation process is based on the number of pixels occupying, either entirely or partially, the boundary of soot particle on the transmission electron microscope (TEM) image (Wentzel et al., 2003). The second one is an ensemble method which has been developed by Brasil et al. (1999) and Oh and Sorensen (1997). The ensemble method estimates D_f manually from a power law fit of a scatter plot of morphology parameters of soot particles shown in the electron microscopic images. Recent studies utilizing the ensemble method have shown that D_f falls with the range of 1.53-1.92 for soot particles freshly emitted by wildfire (China et al., 2013) and is about 1.80 for soot particles collected in polluted air (Y. Y. Wang et al., 2017). According to the works mentioned above, we noticed that the fractal properties were quantitatively analyzed based on the self-similarity of an ensemble of soot particles rather than individual soot particles, which remains an obstacle to simulating individual soot models numerically and to better observing the aging process of soot particles in the atmosphere. Thus, an VISUAL BASIC program was developed by Xiong and Friedlander (2001), which can derive D_f of individual soot particle though the power law relationship between the location of monomers and the number of monomers in a soot particle. However, this requires the operator to spend 20-30 mins to manually measure the required

parameters of each monomer of individual soot aggregates, which is both tedious and time-consuming. Until now, there is no efficient method to quantify the D_f of individual soot particles on electron microscopy. To increase the efficiency in determining the morphology of individual soot particles on electron microscopic images and to take the advantage of recent rapid progress in computer language and image recognition techniques, it is highly desirable to develop an automated method to accurately determine the D_f of individual soot particles.

2 Methods

2.1 Sampling Site

Detailed information of sampling sites of both field observations and laboratory measurements is summarized in Table S1. For the tunnel site, the Wujing road Tunnel is in Tianjin, which is a highly urbanized and densely populated city in northern China with populations of 15 million. Detailed information about the tunnel can be found in Song et al. (2018). Three sampling sites are located at the entrance (34 m from the inlet), midpoint (584 m from the inlet), and exit (115 m from the outlet) of the tunnel. We also collected particles from diesel buses, heavy-duty diesel vehicles and light-duty gasoline vehicles on dynamometers of two motor vehicle inspection facilities in Nanjing, China. For the particles from biomass burning and coal combustion, we performed both field observations and laboratory experiments. Detailed information is summarized in Table S1. For the urban sampling sites, we selected three cities to represent typical urban environments: Beijing in the North China Plain (NCP), Hangzhou in the Yangtze River Delta (YRD) of southern China, and Hong Kong in the Pearl River Delta (PRD) of southern China. These three cities are all metropolises in China with populations of 21.5, 9.8 and 7.5 million, respectively. The sampling sites in Beijing, Hangzhou, and Hong Kong were located in China University of Mining and Technology (Beijing), Zhejiang University, and Hong Kong Polytechnic University, respectively. The two rural sites of Yucheng and Lin'an were definite background sites, far from any cities and surrounded by small villages, hilly lands and cultivated lands.

2.2 Aerosol sampling and analysis

Individual particle samples were collected for 30-180 s on copper (Cu) transmission electron microscopic (TEM) grids covered with carbon film (lacey carbon, SPI supplies lacey carbon

coated, 300 mesh copper grids, 3 mm). A two-stage cascade impactor (DKL-2, Genstar Electronic Technology, China) with a 0.5 mm and 0.3 mm diameter jet nozzle at air flow rate of 1.0 L/min was used to collect aerosol samples. A TEM (JEOL JEM-2100, Japan) coupled with an energy-dispersive X-ray spectrometer (EDS, INCA X-MaxN 80T, Oxford Instruments, United Kingdom) was used to obtain the image and elemental composition of individual particles. Because the distribution of aerosol particles of different size was not uniform on the TEM grids, we chose 3-4 areas from the center to edge of the sampling spot and analyzed all the particles to represent different sized particles.

2.3 Fractal dimension analysis of soot particles

The fractal dimension of soot particle is an important morphological parameter and is mathematically related to other parameters through the scaling law (Brasil et al., 1999; Köylü et al., 1995; Oh & Sorensen, 1997):

$$N = K_g\left(\frac{R_g}{R_0}\right)^{D_f} \quad (1)$$

where D_f is fractal dimension, R_g is the radius of gyration, K_g is fractal prefactor, R_0 represents average radius of the monomer, and N is the number of the primary monomers of the aggregate. The scaling law is the theoretical basis used in the box counting, ensemble, and soot parameters methods considered in this study.

2.4 Box Counting Method

The box counting method, also called the nested square method, is a well-developed method to determine the D_f of individual particles (Lottin et al., 2013). In this study, we use FracLac, which is a plugin for ImageJ software (http://imagej.nih.gov/ij/) to implement the box counting method. The details of the box counting method are provided in the Supporting Information (SI).

2.5 Ensemble Method

The ensemble method, also known as the collective method based on the scaling law, has received increasing attention in recent years (China et al., 2014; Y. Y. Wang et al., 2017). This method first requires parameters of a number of soot aggregates and finally provides a mean D_f of all the particles in the sample through manual efforts. In this method, the fractal dimension and prefactor can be derived from the linear fit of a scatter plot of log(N) versus log(R_g /R_0) based on equation (1). In addition to the D_f, the total number of monomers (N) (Figure 1) and

overlap parameter (δ) of individual soot particles can also be estimated in the ensemble method through equations (2) and (3):

$$N = k_a(\frac{A_a}{A_p})^{\alpha} \quad (2)$$

$$\delta = 2a/l \quad (3)$$

where A_a is the projected area of soot aggregate, A_p is the mean projected area of monomers, k_a is a constant, and α is an empirical projected area exponent. The overlap parameter (δ) dependent on the monomer radius (a) and the distance between the centers of two touching monomers (l)(Oh & Sorensen, 1997). If δ=1, the monomers are in point contact. In addition, R_g in equation (1) can be estimated from the maximum projected length of an aggregate (L_{max}) (Figure 1), using the following relationship (Brasil et al., 1999):

$$L_{max}/2R_g = 1.50 \pm 0.05 \quad (4)$$

Here, L_{max} is an easily measurable parameter based on the TEM image, which can simplify the calculation process. As shown in Figure S2, the soot particles collected in the urban tunnel (sample-A) have a mean $D_f = 1.70$.

2.6 Soot parameters method

Based on equation (1), we developed a novel and accurate algorithm, named the soot parameters (SP) method, programmed with the Python language and based on the scaling law and image recognition technology. The SP method can automatically identify individual soot particles and their monomers in the TEM image and further compute D_f and other morphological parameters (e.g., radius of gyration, fractal prefactor, radius of the monomer) for one single soot particle. Then the SP contains the scaling law equation to further compute D_f of individual soot particle. Here we developed this automated method based on equation (1) without any assumptions for parameters. Figure S3 shows the step-by-step procedure of this approach using a soot particle collected from traffic emissions as an example.

In the code of the SP method, the Otsu algorithm (Kapur et al., 1985; Otsu, 1979), Opening and Closing algorithm (Pitas, 2000), Canny Edge detection (CED) (Canny, 1986), and Circular Hough Transform (CHT) (Duda & Hart, 1972; Hough Paul, 1962) have been used to analyze the features of different particles. The background of TEM images varies sample by sample and image by image due to the differences among the types of particles, carbon film, and the magnification/intensity setting. We first apply Otsu algorithm to implement the image

segmentation and search for a threshold that minimizes the intraclass variances of the segmented image. At the first step, the 16 bits images were converted to 8 bits, as shown in Figure S3b. In order to further eliminate irregularities on the image background, a morphological smoothing operator, called Opening and Closing method, was applied in the SP. At the second step, the CED was applied to detect outlines of monomers of soot aggregates. As shown in Figure S3c, the CED detected the outline of monomers according to the intensity and gradient of the image, which means more contour curves would be detected in darker and more concentrated areas, then result in more monomers recognized during the next process of CHT. Before the CHT, the Python code would display a pop-up window to require selecting the region of interest to distinguish the target soot particle and substrate of carbon films, as shown in Figure S3d. After selection, we got a series of curve fragments of target soot particle, which can be put into the CHT for the monomers detection (Figure S3e). The CHT algorithm is good at detecting circles and has been used to detect soot particle in previous studies (Grishin et al., 2012; Kook et al., 2016). We improved the algorithm of CHT by re-recognizing the monomers twice in large monomers and small monomers, respectively, to ensure that the recognition result is consistent with the human observation. Finally, a PNG image and a CSV file that contains one big data of all the morphology information (e.g., monomer positions, number of monomers, radius of gyration, radius of monomers, and fractal dimension) can be produced. The SP method can automatically complete all the steps without any manual operations except Step 4 shown in Figure S3d.

The basic theory of the SP method is the scaling relationship between the morphology information and the number of monomers in fractal aggregates. So we can obtain the location (x, y) and radius of each monomer (Figure S3f) and the total number of monomers (N) in individual soot particles, which can be used to further derive the radius of gyration (R_g) according to equation (5) (Oh & Sorensen, 1997).

$$R_g = \left(\frac{1}{\sum_0^N m_i} \sum (m_i r_i^2)\right)^{\frac{1}{2}} \quad (5)$$

where r_i is the position vector of the center of the i^{th} monomer, m_i is the mass of the i^{th} monomer. After we obtain the value of R_g, number of monomers and radius of individual soot particle through the SP method, D_f can be derived from the slope of the plot log(N) versus log(R_g/R_0) based on the equation (1).

Note that the monomers overlap in the three-dimensional structure which can cause darkened color from gray to dark on the projection of soot particles in TEM images. The image recognition technique is applied in the SP to detect more monomers in the darker and more complex part of the particles in the process of image recognition algorithm. Moreover, the method can deal with the embedded soot particles in which monomers are engulfed into other materials and not visible from the TEM images (Figure S4a). When processing such invisible part, the SP method packs this part of particles using the monomers with the average monomer diameter and overlapping rate of the recognized monomers, as shown in Figure S4b.

3 Results and Discussion

3.1 Comparisons of soot fractal dimension

Here we compared two box counting methods (i.e., box counting method and sliding box method), SP method, and an ensemble method, using the same set of images that includes 255 soot particles in tunnel sample-A (see Table S2). Figure 2a shows that the average D_f values of soot aggregates from the four methods range from 1.63 to 1.83. The ensemble method yields D_f = 1.70 for the soot particles collected in the tunnel, which generally agrees with D_f calculated by the same method for soot emitted from sources, namely 1.70-1.78 from the spark ignition vehicles engines (Chakrabarty et al., 2006), 1.70-1.85 from diesel (Soewono & Rogak, 2011; Wentzel et al., 2003), 1.52-1.94 from road side (China et al., 2014), and 1.70±0.04 from pre-mixed ethane and oxygen gas combustion (Chakrabarty et al., 2007). Moreover, D_f= 1.70 of soot particles collected in the tunnel fall into the range of freshly emitted soot particles (1.53-1.78) (China et al., 2013) but far less than embedded (fully coated) soot particles (1.9-2.6) (Kouji Adachi et al., 2010; Bambha et al., 2013; Y. Y. Wang et al., 2017) in the urban air. Overall, the measured result is reasonable because the heavy vehicular traffic in the tunnel results in copious amounts of fresh soot particles.

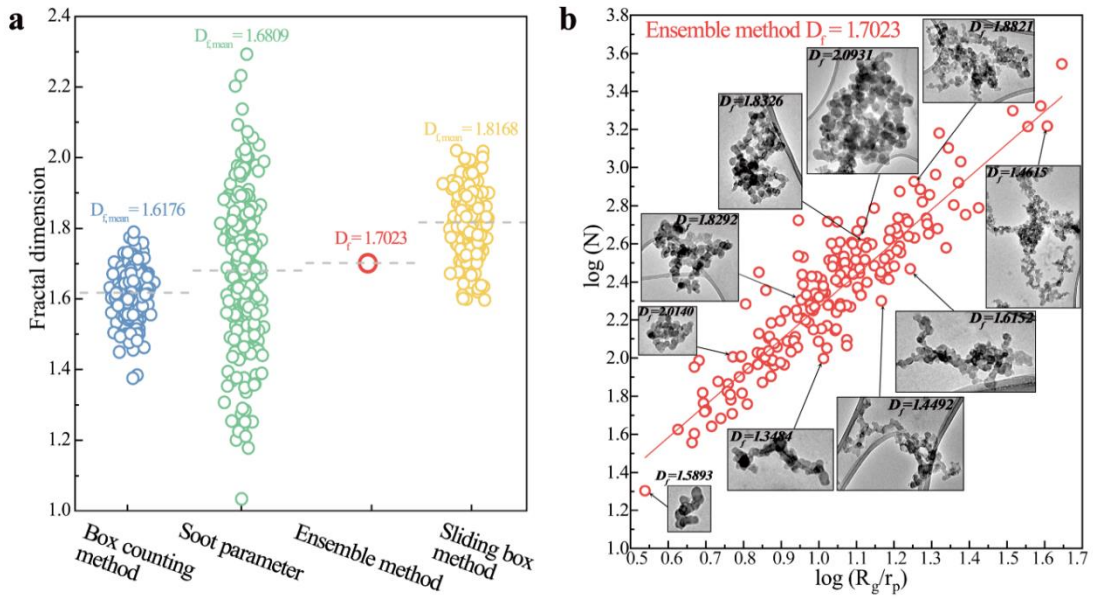

Figure 2. D_f comparisons of soot particles obtained from different methods. (a): Fractal dimensions calculated by box counting method, soot parameter (SP), ensemble method, and sliding box method for the same soot samples collected from traffic emissions in a tunnel. (b): Fractal dimension calculated by the ensemble method (scatter and the single fitting result on the top) and SP method (D_f for each soot aggregate in the box). The TEM images of soot particles and their corresponding D_f derived by the SP are shown.

Figure 2a shows that the D_f values from the two box counting methods, 1.62 and 1.82, are the smallest and the largest among the results of the four methods. Because the computation process of both box methods are based on the number of pixels rather than the actual size of the TEM images (see Figure S1), the derived D_f value highly depends on the resolution of each image. Low resolution images may lead to an overestimation of the projected surface area (Gwaze et al., 2006), which would then result in inaccuracy of the D_f. In the process of image binarization (see Figure S1b), the overlapping and the size information of the monomers are lost. Therefore, the two box counting methods may not be appropriate for aggregates composed of polydisperse monomers, which are generally the case.

The average D_f = 1.68 from the SP is very close to D_f= 1.70 from the ensemble method. Figure 2b displays various morphologies of soot particles and their corresponding D_f values from the SP. The SP method not only obtains the average D_f of all the analyzed soot particles but also distinguishes the D_f of individual soot particles (Figure 2b). The D_f values of soot aggregates

collected in the tunnel range in 1.03 to 2.29 by the SP (Figure 2a). The large D_f range of individual soot particles can be attributed to the different aged vehicles emitting different soot structure (China et al., 2014; Dye et al., 2000; Zhu et al., 2005). On urban roads, there are always different types and ages of private cars.

Based on their data processing and comparisons of their derived D_f values of soot particles, limitations and advantages of all the four methods were summarized in Table S3. The ensemble method cannot differentiate D_f in individual soot particles. Moreover, k_a and α in equation (2) (see Methods) are widely accepted as empirical values in the literature (China et al., 2013; Oh & Sorensen, 1997), and the estimation of δ in equation (3) is also subject to large uncertainty as we cannot figure out the lattice spacing between every pair of monomers in individual soot aggregate. On the contrary, the SP method can directly measure various parameters (e.g., d_p, R_g , N and K_g) in equation (5) and (1) and further calculates the D_f of individual soot particles. The key point is that the SP method can accurately identify polydisperse monomers in individual soot particles (see Figure S3), while the ensemble method can only assume the monomers to be same-sized spheres. However, the SP can better recognize TEM images up to now while the ensemble method can also acquire the information from scanning electron microscope (SEM) images. In a word, we conclude that the SP method is superior based on comparisons between the SP and ensemble methods: it is an automated and highly efficient tool to provide the fractal dimensions of individual soot particles in TEM images.

3.2 Evaluating the SP method

The newly developed SP method consists of image processing and mathmatical calcuations. It is necessary to evaluate how the D_f from the SP method can precisely represent the fractal morphology of soot aggregates. Firstly, we test the image processing in the SP and quantify the ability of automated measurements. It is well known that the size of soot monomers (d_p) is an important parameter to reflect the aggregate structure of individual soot particles (China et al., 2014) and affect the D_f calculation in equation (1). Here we compare the size distribution of soot monomer in all the soot particles in sample-A from the manual measurements and automated identification from the SP method (Figure 3a, 3b).

The size distribution of 48,174 monomers from one big data generated by the SP method shows that the d_p of soot monomer falls in a range of 15-52 nm with a mean size of 27.2 nm,

which is close to the manually determined d_p in a range of 14-65 nm with a mean size of 29.2 nm. The monomer d_p from these two approaches in our study is similar to the soot d_p in a range of 20-40 nm from vehicle emissions of spark ignition engines (Chakrabarty et al., 2006), 26-44 nm from traffic samples in Arizona, and 10-60 nm from a light-duty diesel engine (Zhu et al., 2005). Moreover, assuming that the d_p satisfies the lognormal size distribution, the values of geometric standard deviation (σ_g) obtained by the manual and automated measurements are given in Figure 3a and 3b, which are in good agreement (~1.28) (Figure 3a, 3b). The result falls into a range of 1.11-1.54 for the soot σ_g from ethylene combustion, exhaust of aircraft engines, vehicle emissions, and wood combustion (Bescond et al., 2014; Chakrabarty et al., 2006; Gwaze et al., 2006).

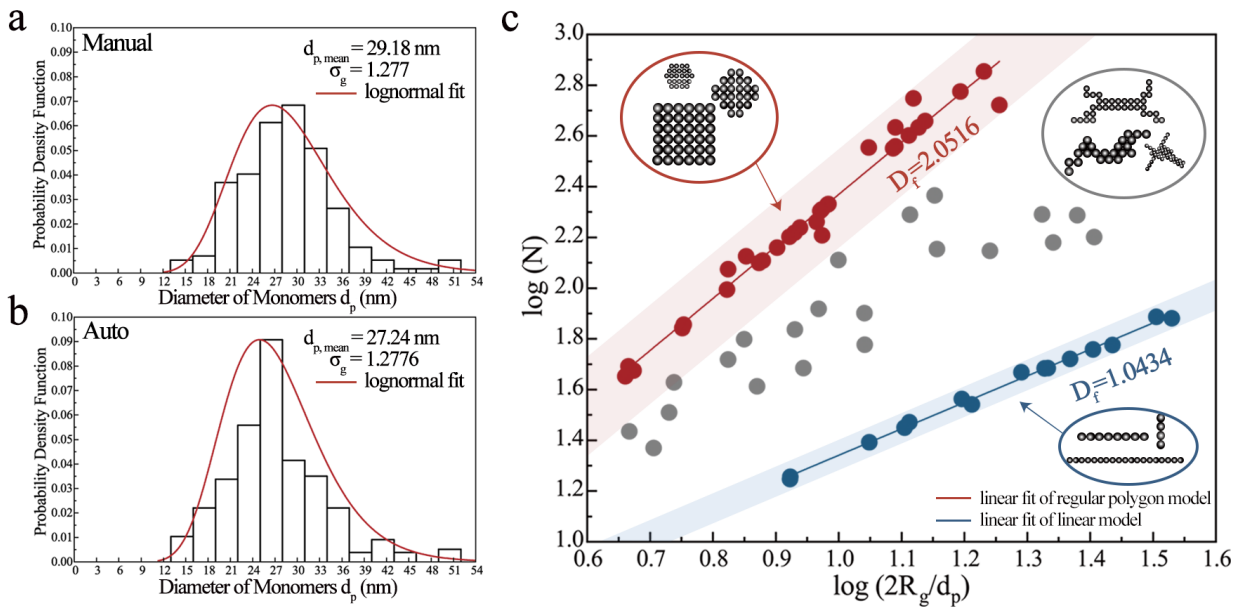

Figure 3. The size distributions of the diameter of monomers (d_p) with the fitted normal distribution (red lines): (a) Manual measurement from the ensemble method, (b) Automated measurement from the SP method, (c) The fractal dimension of linear models (blue), regular polygon models (red), and soot-like models (grey) calculated by the ensemble method.

We constructed well-defined standard aggregates with known D_f based on the scaling law (equation 1). According to the geometric theory, these regular objects have their fixed D_f, i.e., a line has $D_f = 1$, a planar structure has $D_f = 2$, and a cube has $D_f = 3$. To further validate the SP accuracy, two types of standard models were generated: linear chain and regular polygon (Figure 3c). Finally, the SP obtains the D_f from 1.00 to 2.01 of 16 linear models and 29 regular polygon

models, respectively. This shows that the D_f from the SP method is in good agreement with the expected theoretical values. The ensemble method is also used to obtain D_f at 1.04 and 2.05 for the linear and regular polygon models, respectively (Figure 3c). This result shows that the calculated D_f displays a nearly perfect correlation when we consider the standard models with similar shapes. If we generate an ensemble of particles containing some compact and some chain-like models to mimic the real soot particles with different monomer sizes, these D_f data of individual model particles scatter between the linear and polygon models but cannot be fitted by a linear regression. As a result, the accuracy of the ensemble method is significantly reduced if one sample significantly contains different morphologies of soot particles. In other word, the ensemble method can only work well for self-similar soot particles in the sample that all have similar fractal dimensions. Moreover, the ensemble method cannot provide D_f of individual soot particles. On the contrary, the SP can remedy the drawbacks of the ensemble method and provide us with new insight into the calculation and knowledge of the fractal properties of individual soot particles. Moreover, the SP incorporates the automated image processing capability and thus can process a large number of soot aggregates in a short time.

3.3 Morphology characteristics of real soot particles

The soot formation process highly depends on the combustion conditions and the types of combustion sources (Buseck et al., 2014; Zhu et al., 2005). As shown in the TEM images (Figure 4), the monomers, aggregate size, and fractal properties of individual soot particles vary significantly among the particles even in the same sample (Bond et al., 2013). Hence, quantifying the morphology of individual soot-containing particles is critical to understand the feature of emission sources and the aging process of soot particles (China et al., 2013; Y. Y. Wang et al., 2017). We analyzed the morphology and mixing structure of individual soot-containing particles through transmission electron microscopy (TEM) coupled with energy dispersive X-ray spectroscopy (EDS). EDS can determine elemental composition of soot-containing particle to assist us in selecting the mixing structure categories. We basically judge the mixing structure categories through the TEM observations. It should be noted that the method has been well used in Y. Wang et al. (2021a) through the volume proportion of BC embedded in coating. Based on the TEM/EDS, we simply classified the soot particles into three types: bare-like, partly-coated, and embedded. The bare-like soot is a chain-like aggregate with no or extremely thin organic matter (OM) coating (Figure 4a). The partly-coated soot represents

a soot particle that is partly mixed with organic or inorganic components (Figure 4b). The embedded soot particle is heavily coated or entirely embedded within other aerosols (Figure 4c). Through the functions of image recognition techniques, the SP method can still obtain parameters of monomers even for soot particles covered by secondary aerosols (e.g., sulfate, nitrate, and organic matter) in TEM images (Figure 4). Figure 4 shows the three different types of soot particles collected from traffic emissions in the tunnel (sample-B) and their D_f calculated by the SP, such as D_f= 1.50 of a bare-like, D_f = 1.66 of a partly coated, and D_f = 1.79 of an embedded soot particle.

As the most important parameter to quantify the morphology of soot particles, the D_f plays an important role in the evaluation of the scattering and radiative properties of soot particles (Li Liu & Mishchenko, 2005; Y. Wang et al., 2021b). Figure 4 shows that soot monomers are identified accurately by the green circles in the TEM images. The parameters of position and size of every monomer are used in the calculation of the D_f for each soot aggregate. The number, position, size, and D_f of soot monomers are then used to generate a three-dimensional numerical model of each soot aggregate. Based on parameters such as D_f, k_g, and N of individual soot particles in TEM images and the results from EDS, the structure of a soot aggregate was generated by a tunable algorithm proposed by Filippov et al. (2000) and the detailed information about how to construct the soot models is described by Y. Wang et al. (2021a) and Y. Wang et al. (2021b). Based on their morphological parameters from the SP, we successfully generate for the first time three numerical soot models (Figure 4). Once the numerical soot models are built, they can be further fed to the optical models (e.g. DDA and T-matrix) to calculate the optical properties of soot particles (Kouji Adachi et al., 2010; Kahnert & Devasthale, 2011; Y. Wang et al., 2021b; Zeng et al., 2019).

3.4 Quantifying the aging process of soot particles

We noticed that the morphology of individual soot particles varied significantly. To trace the aging process and the fractal properties of soot particles, we further measured the D_f of soot particles from the same emission source (see Sample-B, Table S2) using the SP in a tunnel. Figure S5 shows that D_f varies with the location in the tunnel, such as 1.61±0.19 in the tunnel entrance, 1.66±0.19 in the tunnel midpoint, and 1.70±0.15 in the tunnel exit. The increased D_f from the tunnel entrance to the tunnel exit is consistent with the change of mixing structure of

soot particles (Figure S5), suggesting that some soot particles become slightly aged in the 1554 m tunnel. Based on the sampling time, the aging ratio is estimated to be 0.18/h (aging ratio = ($D_{f,\ exit} - D_{f,\ entrance}$)/$\Delta t$) in the tunnel based on the D_f changes.

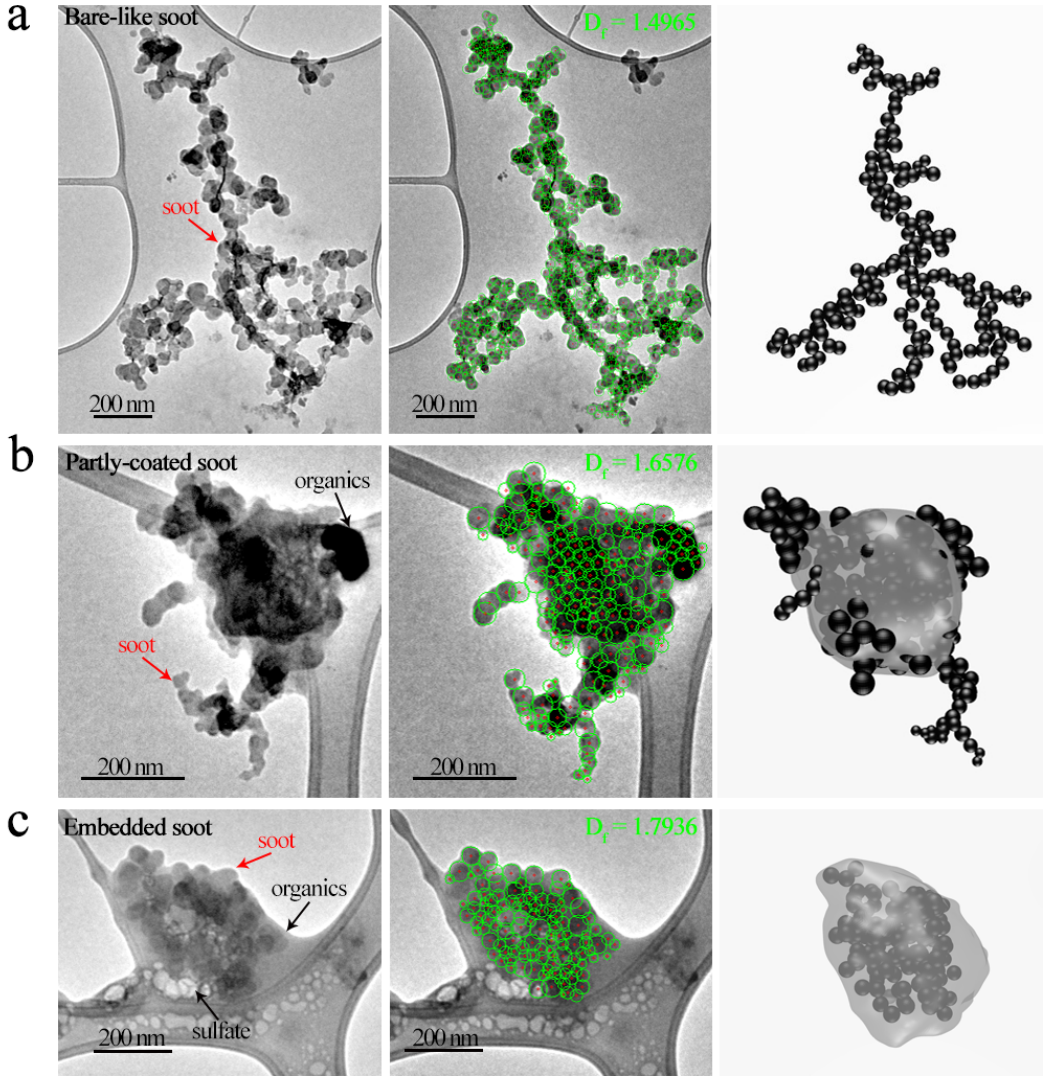

Figure 4. TEM images of three typical soot particles (first column), their corresponding SP processed images (second column), and their three-dimension models (third column). (a) One fresh soot particle collected at the tunnel entrance and its D_f = 1.50, (b) Partly-coated soot particle collected at the tunnel midpoint and its D_f = 1.66, (c) Embedded soot particle collected at the tunnel exit and its D_f = 1.79. The 3D soot numerical models are generated from a tunable algorithm (Filippov et al., 2000) and one EMBS developed by Y. Wang et al. (2021a) based on the D_f of soot particles and the numbers and sizes of monomers.

1,370 soot particles from three combustion sources — vehicles, biomass burning, and coal burning — and five ambient sampling sites (e.g., Beijing city, Hangzhou city, Hong Kong city, Lin'an rural site and Yucheng rural site) were analyzed. Figure 5 shows that the average D_f values of various soot particles are 1.66 for vehicles, 1.75 for biomass burning, 1.76 for coal burning, 1.77 for urban air, and 1.85 for rural air. The majority soot particles from vehicles, biomass burning, and coal burning are partly-coated soot particles with the mean D_f of 1.73, 1.77 and 1.79, respectively. The mean D_f values of bare-like soot particles in the corresponding combustion sources are 1.54, 1.57, and 1.58, respectively (Figure 5). We also found that the amount of embedded soot particles is nearly the same as that of partly-coated soot particles from both the biomass burning and coal burning sources, which have the same D_f at 1.86. The high percentage of organic aerosols emitted from biomass burning and coal burning (Hodshire et al., 2019; Lei Liu et al., 2017; Zhang et al., 2018) may have contributed to the presence of large amount of embedded soot particles.

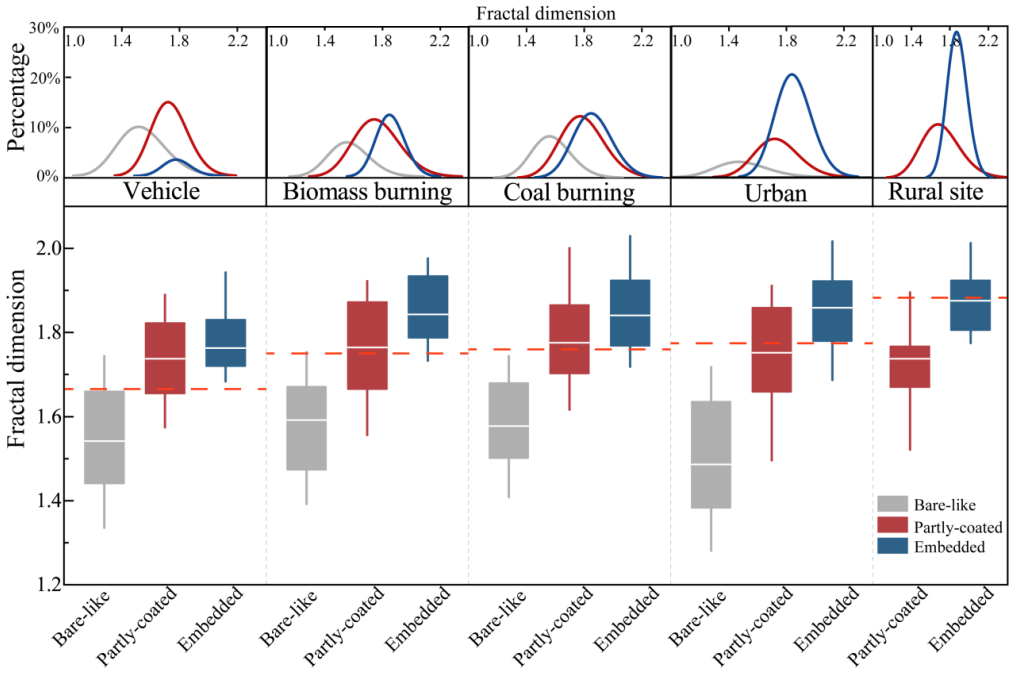

Figure 5. D_f of three types of soot particles from vehicle exhaust, biomass burning, coal burning, and from urban and rural ambient air. The white lines in the boxes are the medians, and the red dashed lines display the mean D_f of soot particles from those sources. Vertical error bars represent the 90% confidence interval of D_f. The percentages of the three types of soot particles are shown above the box plots.

Compared with the soot particles from the combustion sources, the D_f values of soot particles from urban sites (1.77) and rural sites (1.85) were larger, and no bare-like soot particle was found at the remote rural sites. These results suggest that the aging process during the transport from emission sources to ambient air result in more compact soot particles. Coatings of secondary aerosols significantly changed the fractal morphology of soot particles from the chain-like aggregate to more compact one. Moreover, we noticed that the number fraction of embedded soot particles at the rural sites was significantly higher and that they had the highest D_f at 1.88, suggesting that the long-range-transport of aerosol particles could transform the relatively open structure of freshly emitted soot particles to a more compact structure (Khalizov et al., 2009; Pei et al., 2018; Y. Y. Wang et al., 2017).

In summary, we provide a novel method to automatically determine the fractal properties of individual soot particles. This method opens a new door for the microscopic characterization of individual soot particles. It will transform the way to characterize the morphology of soot particles and enable a better understanding of the soot aging process.

Acknowledgments

Funding Sources

This work was funded by the National Natural Science Foundation of China (42075096; 91844301) and Zhejiang Provincial Natural Science Foundation of China (LZ19D050001).

Author Contributions

Y.P. and W.L. designed this study and wrote the original draft. Y.W. and Y.Z. collected the aerosol particles. Y.P., Z.W., L.L., Y.W. and Y.Z. carried out the laboratory experiments and data analyses. S. K., F. L., and Z.S. interpreted the results and improved the manuscript

Conflict of Interest

The authors declare no conflicts of interest relevant to this study.

Data Availability Statement

Data supporting the results are available in the supporting information. The data presented in this publication are available online (https://10.6084/m9.figshare.17871755). The codes are available from website https://doi.org/10.6084/m9.figshare.16393833

References

Adachi, K., Chung S. H.,Buseck P. R. (2010), Shapes of soot aerosol particles and implications for their effects on climate, *Journal of Geophysical Research: Atmospheres*, *115*(D15), D15206, https://doi.org/10.1029/2009JD012868

Adachi, K., Chung S. H., Friedrich H.,Buseck P. R. (2007), Fractal parameters of individual soot particles determined using electron tomography: Implications for optical properties, *Journal of Geophysical Research: Atmospheres*, *112*(D14), D14202, https://doi.org/10.1029/2006JD008296

Bambha, R. P., Dansson M. A., Schrader P. E.,Michelsen H. A. (2013), Effects of volatile coatings and coating removal mechanisms on the morphology of graphitic soot, *Carbon*, *61*, 80-96, https://doi.org/https://doi.org/10.1016/j.carbon.2013.04.070

Bescond, A., Yon J., Ouf F. X., Ferry D., Delhaye D., Gaffie D., et al. (2014), Automated Determination of Aggregate Primary Particle Size Distribution by TEM Image Analysis: Application to Soot, *Aerosol Science and Technology*, *48*(8), 831-841, https://doi.org/10.1080/02786826.2014.932896

Bond, T. C., Doherty S. J., Fahey D. W., Forster P. M., Berntsen T., DeAngelo B. J., et al. (2013), Bounding the role of black carbon in the climate system: A scientific assessment, *Journal of Geophysical Research: Atmospheres*, *118*(11), 5380-5552, https://doi.org/10.1002/jgrd.50171

Boucher, O., D. Randall, P. Artaxo, C. Bretherton, G. Feingold, P. Forster, et al. (2013), Clouds and Aerosols, paper presented at *Climate Change 2013: The Physical Science Basis. Contribution of Working Group I to the Fifth Assessment Report of the Intergovernmental Panel on Climate Change*, Cambridge Univ. Press, New York.

Brasil, A. M., Farias T. L.,Carvalho M. G. (1999), A recipe for image characterization of fractal-like aggregates, *Journal of Aerosol Science*, *30*(10), 1379-1389, https://doi.org/10.1016/S0021-8502(99)00026-9

Buseck, P. R., Adachi K., Gelencsér A., Tompa É.,Pósfai M. (2014), Ns-Soot: A Material-Based Term for Strongly Light-Absorbing Carbonaceous Particles, *Aerosol Science and Technology*, *48*(7), 777-788, https://doi.org/10.1080/02786826.2014.919374

Canny, J. F. (1986), A Computational Approach to Edge Detection. In Fischler, et al. (Eds.), *Readings in Computer Vision*, (pp. 679-698), Morgan Kaufmann, San Francisco

Chakrabarty, R. K., Moosmüller H., Arnott W. P., Garro M. A., Slowik J. G., Cross E. S., et al. (2007), Light scattering and absorption by fractal-like carbonaceous chain aggregates: comparison of theories and experiment, *Applied Optics*, *46*(28), 6990-7006, https://doi.org/10.1364/AO.46.006990

Chakrabarty, R. K., Moosmüller H., Arnott W. P., Garro M. A.,Walker J. (2006), Structural and Fractal Properties of Particles Emitted from Spark Ignition Engines, *Environmental Science & Technology*, *40*(21), 6647-6654, https://doi.org/10.1021/es060537y

China, S., Mazzoleni C., Gorkowski K., Aiken A. C.,Dubey M. K. (2013), Morphology and mixing state of individual freshly emitted wildfire carbonaceous particles, *Nature Communications*, *4*, 2122, https://doi.org/10.1038/ncomms3122

China, S., Salvadori N.,Mazzoleni C. (2014), Effect of Traffic and Driving Characteristics on Morphology of Atmospheric Soot Particles at Freeway On-Ramps, *Environmental Science & Technology*, *48*(6), 3128-3135, https://doi.org/10.1021/es405178n

Ding, A. J., Huang X., Nie W., Sun J. N., Kerminen V. M., Petäjä T., et al. (2016), Enhanced haze pollution by black carbon in megacities in China, *Geophysical Research Letters*, *43*(6), 2873-2879, https://doi.org/10.1002/2016GL067745

Duda, R. O.,Hart P. E. (1972), Use of the Hough transformation to detect lines and curves in pictures, *Commun. ACM*, *15*(1), 11–15, https://doi.org/10.1145/361237.361242

Dye, A. L., Rhead M. M.,Trier C. J. (2000), The quantitative morphology of roadside and background urban aerosol in Plymouth, UK, *Atmospheric Environment*, *34*(19), 3139-3148, https://doi.org/10.1016/S1352-2310(99)00437-9

Filippov, A. V., Zurita M.,Rosner D. E. (2000), Fractal-like aggregates: Relation between morphology and physical properties, *Journal of Colloid and Interface Science*, *229*(1), 261-273, https://doi.org/10.1006/jcis.2000.7027

Grishin, I., Thomson K., Migliorini F.,Sloan J. J. (2012), Application of the Hough transform for the automatic determination of soot aggregate morphology, *Applied Optics*, *51*(5), 610-620, https://doi.org/10.1364/Ao.51.000610

Gwaze, P., Schmid O., Annegarn H. J., Andreae M. O., Huth J.,Helas G. (2006), Comparison of three methods of fractal analysis applied to soot aggregates from wood combustion, *Journal of Aerosol Science*, *37*(7), 820-838, https://doi.org/10.1016/j.jaerosci.2005.06.007

Hodshire, A. L., Bian Q., Ramnarine E., Lonsdale C. R., Alvarado M. J., Kreidenweis S. M., et al. (2019), More Than Emissions and Chemistry: Fire Size, Dilution, and Background Aerosol Also Greatly Influence Near-Field Biomass Burning Aerosol Aging, *124*(10), 5589-5611, https://doi.org/10.1029/2018JD029674

Hough Paul, V. C. (1962), Method And Means For Recognizing Complex Patterns, edited, HOUGH PAUL V C, US,

Ishimoto, H., Kudo R.,Adachi K. (2019), A shape model of internally mixed soot particles derived from artificial surface tension, *Atmos. Meas. Tech.*, *12*(1), 107-118, https://doi.org/10.5194/amt-12-107-2019

Johansson, K. O., Head-Gordon M. P., Schrader P. E., Wilson K. R.,Michelsen H. A. (2018), Resonance-stabilized hydrocarbon-radical chain reactions may explain soot inception and growth, *Science*, *361*(6406), 997, https://doi.org/10.1126/science.aat3417

Kahnert, M.,Devasthale A. (2011), Black carbon fractal morphology and short-wave radiative impact: a modelling study, *Atmospheric Chemistry and Physics*, *11*(22), 11745-11759, https://doi.org/10.5194/acp-11-11745-2011

Kapur, J. N., Sahoo P. K.,Wong A. K. C. (1985), A new method for gray-level picture thresholding using the entropy of the histogram, *Computer Vision, Graphics, and Image Processing*, *29*(3), 273-285, https://doi.org/10.1016/0734-189X(85)90125-2

Khalizov, A. F., Zhang R., Zhang D., Xue H., Pagels J.,McMurry P. H. (2009), Formation of highly hygroscopic soot aerosols upon internal mixing with sulfuric acid vapor, *114*(D5), https://doi.org/https://doi.org/10.1029/2008JD010595

Kook, S., Zhang R. L., Chan Q. N., Aizawa T., Kondo K., Pickett L. M., et al. (2016), Automated Detection of Primary Particles from Transmission Electron Microscope (TEM) Images of Soot Aggregates in Diesel Engine Environments, *Sae International Journal of Engines*, *9*(1), 279-296, https://doi.org/10.4271/2015-01-1991

Köylü, Ü. Ö., Faeth G. M., Farias T. L.,Carvalho M. G. (1995), Fractal and projected structure properties of soot aggregates, *Combustion and Flame*, *100*(4), 621-633, https://doi.org/10.1016/0010-2180(94)00147-K

Li, J., Anderson J. R.,Buseck P. R. (2003), TEM study of aerosol particles from clean and polluted marine boundary layers over the North Atlantic, *Journal of Geophysical Research: Atmospheres*, *108*(D6), 4189, https://doi.org/10.1029/2002JD002106

Liu, L., Kong S., Zhang Y., Wang Y., Xu L., Yan Q., et al. (2017), Morphology, composition, and mixing state of primary particles from combustion sources — crop residue, wood, and solid waste, *Scientific reports*, *7*(1), 5047, https://doi.org/10.1038/s41598-017-05357-2

Liu, L.,Mishchenko M. I. (2005), Effects of aggregation on scattering and radiative properties of soot aerosols, *Journal of Geophysical Research: Atmospheres*, *110*(D11), D11211, https://doi.org/10.1029/2004JD005649

Lottin, D., Ferry D., Gay J. M., Delhaye D.,Ouf F. X. (2013), On methods determining the fractal dimension of combustion aerosols and particle clusters, *Journal of Aerosol Science*, *58*, 41-49, https://doi.org/10.1016/j.jaerosci.2012.12.009

Moffet, R. C.,Prather K. A. (2009), In-situ measurements of the mixing state and optical properties of soot with implications for radiative forcing estimates, *Proceedings of the National Academy of Sciences of the United States of America*, *106*(29), 11872-11877, https://doi.org/10.1073/pnas.0900040106

Oh, C.,Sorensen C. M. (1997), The effect of overlap between monomers on the determination of fractal cluster morphology, *Journal of Colloid and Interface Science*, *193*(1), 17-25, https://doi.org/10.1006/jcis.1997.5046

Otsu, N. (1979), A Threshold Selection Method from Gray-Level Histograms, *IEEE Transactions on Systems, Man, and Cybernetics*, *9*(1), 62-66, https://doi.org/10.1109/TSMC.1979.4310076

Pei, X., Hallquist M., Eriksson A. C., Pagels J., Donahue N. M., Mentel T., et al. (2018), Morphological transformation of soot: investigation of microphysical processes during the condensation of sulfuric acid and limonene ozonolysis product vapors, *Atmospheric Chemistry and Physics*, *18*(13), 9845-9860, https://doi.org/10.5194/acp-18-9845-2018

Pendergrass, A. G.,Hartmann D. L. (2012), Global-mean precipitation and black carbon in AR4 simulations, *Geophysical Research Letters*, *39*(1), L01703, https://doi.org/10.1029/2011GL050067

Peng, J. F., Hu M., Guo S., Du Z. F., Zheng J., Shang D. J., et al. (2016), Markedly enhanced absorption and direct radiative forcing of black carbon under polluted urban environments, *Proceedings of the National Academy of Sciences of the United States of America*, *113*(16), 4266-4271, https://doi.org/10.1073/pnas.1602310113

Pitas, I. (2000), *Digital Image Processing Algorithms and Applications*, Wiley-Interscience, New York.

Ramanathan, V.,Carmichael G. (2008), Global and regional climate changes due to black carbon, *Nature Geoscience*, *1*(4), 221-227, https://doi.org/10.1038/ngeo156

Soewono, A.,Rogak S. (2011), Morphology and Raman Spectra of Engine-Emitted Particulates, *Aerosol Science and Technology*, *45*(10), 1206-1216, https://doi.org/10.1080/02786826.2011.587036

Song, C., Ma C., Zhang Y., Wang T., Wu L., Wang P., et al. (2018), Heavy-duty diesel vehicles dominate vehicle emissions in a tunnel study in northern China, *Science of the Total Environment*, *637-638*, 431-442, https://doi.org/10.1016/j.scitotenv.2018.04.387

Teng, S., Liu C., Schnaiter M., Chakrabarty R. K.,Liu F. (2019), Accounting for the effects of nonideal minor structures on the optical properties of black carbon aerosols, *Atmospheric Chemistry and Physics*, *19*(5), 2917-2931, https://doi.org/10.5194/acp-19-2917-2019

van Poppel, L. H., Friedrich H., Spinsby J., Chung S. H., Seinfeld J. H.,Buseck P. R. (2005), Electron tomography of nanoparticle clusters: Implications for atmospheric lifetimes and radiative forcing of soot, *Geophysical Research Letters*, *32*(24), L24811, https://doi.org/10.1029/2005GL024461

Wang, Y., Li W., Huang J., Liu L., Pang Y., He C., et al. (2021a), Nonlinear enhancement of radiative absorption by black carbon in response to particle mixing structure, *Geophysical Research Letters*, *48*(24), e2021GL096437, https://doi.org/https://doi.org/10.1029/2021GL096437

Wang, Y., Pang Y., Huang J., Bi L., Che H., Zhang X.,Li W. (2021b), Constructing Shapes and Mixing Structures of Black Carbon Particles With Applications to Optical Calculations, *Journal of Geophysical Research: Atmospheres*, *126*(10), e2021JD034620, https://doi.org/10.1029/2021JD034620

Wang, Y. Y., Liu F. S., He C. L., Bi L., Cheng T. H., Wang Z. L., et al. (2017), Fractal Dimensions and Mixing Structures of Soot Particles during Atmospheric Processing, *Environmental Science & Technology Letters*, *4*(11), 487-493, https://doi.org/10.1021/acs.estlett.7b00418

Wentzel, M., Gorzawski H., Naumann K. H., Saathoff H.,Weinbruch S. (2003), Transmission electron microscopical and aerosol dynamical characterization of soot aerosols, *Journal of Aerosol Science*, *34*(10), 1347-1370, https://doi.org/https://doi.org/10.1016/S0021-8502(03)00360-4

Xiong, C.,Friedlander S. K. (2001), Morphological properties of atmospheric aerosol aggregates, *Proceedings of the National Academy of Sciences of the United States of America*, *98*(21), 11851-11856, https://doi.org/10.1073/pnas.211376098

Zeng, C., Liu C., Li J., Zhu B., Yin Y.,Wang Y. (2019), Optical Properties and Radiative Forcing of Aged BC due to Hygroscopic Growth: Effects of the Aggregate Structure, *Journal of Geophysical Research: Atmospheres*, *124*(8), 4620-4633, https://doi.org/10.1029/2018JD029809

Zhang, Y., Yuan Q., Huang D., Kong S., Zhang J., Wang X., et al. (2018), Direct Observations of Fine Primary Particles From Residential Coal Burning: Insights Into Their Morphology, Composition, and Hygroscopicity, *Journal of Geophysical Research: Atmospheres*, *123*(22), 12,964-912,979, https://doi.org/10.1029/2018JD028988

Zhu, J., Lee K. O., Yozgatligil A.,Choi M. Y. (2005), Effects of engine operating conditions on morphology, microstructure, and fractal geometry of light-duty diesel engine particulates, *Proceedings of the Combustion Institute*, *30*(2), 2781-2789, https://doi.org/https://doi.org/10.1016/j.proci.2004.08.232